



Impact of crop field burning and mountains on heavy haze in the North China Plain: A case study

X. Long^{1,2}, X. X. Tie^{1,3,4,*}, J. J. Cao^{1,5}, R. J. Huang^{1,6,*}, T. Feng¹, N. Li^{1,7}, S. Y. Zhao¹, J. Tian¹, G. H. Li¹, Q. Zhang⁸

5 ¹Key Lab of Aerosol Chemistry & Physics, SKLLQG, Institute of Earth Environment, Chinese Academy of Sciences, Xi'an, 710061, China

²University of Chinese Academy of Sciences, Beijing, 100049, China

³CAS Center for Excellence in Urban Atmospheric Environment, Xiamen, China

⁴National Center for Atmospheric Research, Boulder, CO, 80303, USA

10 ⁵Institute of Global Environmental Change, Xi'an Jiaotong University, Xi'an, 710049, China

⁶Laboratory of Atmospheric Chemistry, Paul Scherrer Institute (PSI), 5232 Villigen, Switzerland.

⁷Department of Atmospheric Science, National Taiwan University, Taipei, 10617, Taiwan

⁸Center for Earth System Science, Tsinghua University, Beijing, 100084, China

Correspondence to: X. X. Tie (xxtie@urcar.edu) R. J. Huang (rujin.huang@ieecas.cn)



Abstract. Crop field burning (CFB) has important effects on air pollution in China, but it is seldom quantified and reported in a regional scale, which is of great importance for the control strategies of CFB in China, especially in the North China Plain (NCP). With the provincial statistical data and open crop fires captured by satellite (MODIS), we extracted a detailed emission inventory of CFB during a heavy haze event from 6th to 12th October 2014. A regional dynamical and chemical model (WRF-Chem) was applied to investigate the impact of CFB on air pollution in NCP. The model simulations were compared with the in situ measurements of PM_{2.5} (particular matter with radius less than 2.5 μm) concentrations. The model evaluation shows that the correlation coefficients (R) between measured and calculated values exceeds 0.80 and absolute normalized mean bias (NMB) is no more than 14%. In addition, the simulated meteorological parameters such as winds and planetary boundary layer height (PBLH) are also in good agreement with observations. The model was intensive used to study (1) the impacts of CFB and (2) the effect of mountains on regional air quality. The results show that the CFB occurred in southern NCP (SNCP) had significant effect on PM_{2.5} concentrations locally, causing a maximum of 35% PM_{2.5} increase in SNCP. Because of south wind condition, the CFB pollution plume is subjective a long transport to northern NCP (NNCP-with several mega cities, including Beijing of the capital city in China), where there are no significant CFB occurrences, causing a maximum of 32% PM_{2.5} increase in NNCP. As a result, the heavy haze in Beijing is enhanced by the CFB occurred in SNCP. Further more, there are two major mountains located in the western and northern NCP. Under the south wind condition, these mountains play important roles in enhancing the PM_{2.5} pollution in NNCP through the blocking and guiding effects. This study suggests that the PM_{2.5} emissions in SNCP region should be significantly limited in order to reduce the occurrences of heavy haze events in NNCP region, including the Beijing City.

Key words: crop field burning; mountain affect; PM_{2.5} pollution; WRF-Chem; North China Plain (NCP)



1 Introduction

Biomass burning processes contribute large amounts of particulate matter to air pollution (He et al., 2015b; van der Werf et al., 2006). Crop field burning (CFB) is important for biomass burning (Yevich and Logan, 2003), especially in agricultural countries such as China, the CFB accounts for a high proportion of open fires and represents a severe threat to air quality (Cao et al., 2008). Indeed, CFB have already been banned, but the local enforcement of regulation is limited (Zhang and Cao, 2015). Large amounts of crop residues are still burned during the post-harvest seasons (Yan et al., 2006; Streets et al., 2003), and extensive crop fires are concentrated in the North China Plain (NCP) (Huang et al., 2012), where have been frequently suffering haze events in recent years (Yang et al., 2015; Jiang et al., 2015; Wang et al., 2013; Wang et al., 2012).

Previous studies have reported the importance of CFB contribution to $PM_{2.5}$ of the Pearl River delta (PRD) (Wang et al., 2007; Zhang et al., 2010; He et al., 2011), the Yangtze River delta (YRD) (Cheng et al., 2014) and the NCP region (Wang et al., 2007; Li et al., 2010; Cheng et al., 2013; Yang et al., 2015). The impact of CFB is regional, and inter-province transported air pollutants significantly affects regional $PM_{2.5}$ levels and air quality (Cheng et al., 2014). A recent study reports that CFB and regional transport partly illustrates the key process of haze formation in October 2014, especially on Oct. 6th (Yang et al., 2015), but it is lack of study for the quantitative effect. However, related quantification studies are of great importance for the control strategies of CFB in China.

In this study, we analyzed a heavy haze episode occurred in NCP region from "LT" 12:00 6th to 00:00 12th October in 2014, during which CFB were captured by Moderate Resolution Imaging Spectroradiometer (MODIS). Meanwhile, the location and topographic feature of NCP provide a good opportunity to study the impact of mountains on the air pollution. We aims to: (1) analyze the characteristics of the air pollution based on $PM_{2.5}$ concentration; (2) extract a more detailed CFB emission inventory with higher temporal/spatial resolution based on the provincial statistical data and MODIS observations; (3) quantify the contributions of CFB on the evolution of $PM_{2.5}$ concentration and (4) study the effect of mountains (especially the Taihang Mountains and Yanshan Mountains) on the pollution transport during the haze episodes.



2 Description of data

2.1 Geographical Location

In order to study the effect of CFB on local and regional air pollution, the research domain locates in eastern China, covering a large regional area (more than 10 provinces) (see **Fig. 1a**). The NCP region is in the middle of the research domain, with two mountains in the north and west. The Yanshan Mountains locate in the north of NCP with east-west directions, and the Taihang Mountains locate in the west of NCP with southwest-northeast directions (**Fig. 1b**). **Figure 1c** displays the distribution of online sampling sites and CFB captured by MODIS during the haze episodes. According to crop fires, topographic conditions, industrial and agricultural developments, we defined two regions. One is the north part of NCP (NNCP), including two mega cities (Beijing and Tianjin), and the north part of Hebei province, where only few CFB occurred. Another is the south part of the NCP (SNCP), where substantial crop fires occurred during the haze episodes (as shown in **Fig. 1c**). Because of the severe haze problem in the capital city of China (Beijing), one of the main focuses is to study the long-range transport of CFB from SNCP to NNCP.

2.2 PM_{2.5} Measurements

The hourly PM_{2.5} mass concentration were continually monitored by the Ministry of Environmental Protection (MEP) of China (<http://datacenter.mep.gov.cn>), including 5 sites in NNCP and 7 sites in SNCP (indicated by green crosses in **Fig. 1c**). The data was updated from the website: <http://www.pm25.in/>. **Table 1** summarizes the site information and the measured PM_{2.5} concentrations. During the study period, the averaged PM_{2.5} concentrations are 200.0 $\mu\text{g m}^{-3}$ and 184.1 $\mu\text{g m}^{-3}$ in NNCP and SNCP, respectively. The measured PM_{2.5} concentrations are much higher than class II standard (daily mean of 75 $\mu\text{g m}^{-3}$), indicating an occurrence of heavy pollution event. It is worth to note that the highest PM_{2.5} concentrations occurred along the foothill of the Taihang Mountains. For example, at the sites of BJ, BD, SJZ and XT, PM_{2.5} concentrations are 245.5, 287.7, 257.9, and 320.1 $\mu\text{g m}^{-3}$, respectively. The mean PM_{2.5} concentration in these 4 sites is 277.8 $\mu\text{g m}^{-3}$, much higher than 147.2 $\mu\text{g m}^{-3}$ averaged from the other sites.

2.3 Meteorological conditions

The reanalysis meteorological data, including wind direction, wind speed and planetary boundary layer



height (PBLH) were obtained from the European Centre for Medium-range Weather Forecasts (ECMWF), with a spatial resolution of $0.125^\circ \times 0.125^\circ$. The data is available at: <http://www.ecmwf.int/products/data/>. The averaged wind directions and wind speed are displayed in **Table 1**. It shows that during the haze episode, the mean wind directions are 174.8° in NNCP 165.2° in SNCP, and the average wind speeds are 2.4 m s^{-1} in both NNCP and SNCP. The meteorological data suggests that the prevailing winds are continually southerly winds, with weak wind speeds, which are in favor to form haze events. The south winds led to pollution transport from SNCP to NNCP, and generally produced high air pollutions in the Beijing City (Tie et al., 2015).

3 Methods

10 3.1 Model description

The Weather Research and Forecasting Chemical model (WRF-Chem) was used to simulate the spatial and temporal variability of $\text{PM}_{2.5}$ concentration. The WRF-Chem model is a state-of-the-art regional dynamical/chemical transport model with detailed description available at <https://www2.aocom.ucar.edu/wrf-chem>. The model configuration includes simultaneous calculation of dynamical parameters (winds, temperature, boundary layer, clouds, etc.), transport (advective, convective, and diffusive), dry deposition (Wesely, 1989), wet deposition, gas phase chemistry, radiation and photolysis (Tie et al., 2003; Madronich and Flocke, 1999), and online calculation of biogenic emission (Guenther et al., 1994). The gas-phase chemistry was represented in the model by the modified RADM2 (Regional Acid Deposition Model, version 2) gas-phase chemical mechanism (Stockwell et al., 1990; Chang et al., 1987). In the present study, we used the CMAQ (version 4.6) aerosol module developed by US EPA (Binkowski and Roselle, 2003). We also used the Yonsei University (YSU) PBL scheme, which utilizes counter-gradient terms to represent fluxes and explicitly considers the entrainment effect to calculate the PBL heights (Hong et al., 2006). Meanwhile, the model employed the Lin microphysics scheme (Lin et al., 1983), the Noah land-surface model (Chen and Dudhia, 2001), the long-wave radiation parameterization (Mlawer et al., 1997), and the shortwave radiation parameterization (Dudhia, 1989). The model has been successfully applied in several regional pollution studies in the globe (Tie et al., 2009; Tie et al., 2007; He et al., 2015a).

The model resolution is $6 \times 6 \text{ km}$ in $1200 \times 1800 \text{ km}$ domain centered in (117°E , 39°N). Vertical layers



extended from the surface to 50 hPa, with 28 vertical layers, involving 7 layers in the bottom of 1 km. The meteorological initial and boundary conditions were gathered from NCEP FNL Operational Global Analysis data. The lateral chemical initial conditions were constrained by a global chemical transport model-MOZART4 (Model for Ozone and Related chemical Tracers, Version 4) 6-hour output
5 (Emmons et al., 2010;Tie et al., 2005). For the episode simulations, the spin-up time of the WRF-Chem model is 12 hours.

The surface emission inventory used in this study was obtained from the Multi-resolution Emission Inventory for China (MEIC) (Zhang et al., 2009), which is an update and improvement for the year 2010 (<http://www.meicmodel.org>). The emission inventory estimated only anthropogenic emission
10 such as non-residential sources (transportation, agriculture, industry and power) and residential sources related to fuel combustions, we added emission from CFB in the present study.

3.2 Crop field burning emission

To estimate the CFB, we analyzed the annual and monthly number of crop fire events captured by MODIS in the research domain from 2006 to 2014. In the NCP region, the CFB is gradually increasing
15 since 2008, from the minimum fire events of 12, 000 times in 2008 to 27, 000 times in 2014 (**Fig. 2a**), suggesting that the CFB is not efficiently controlled in the region. The burning events mostly occurred in June and October due to the post-harvest activities (**Fig. 2b**). The strong seasonal variation suggests that the emission from CFB is very important, but only occurred in particular months (June and Oct.) to the pollution events in NCP. In order to have the detailed horizontal distribution of the pollutant
20 emissions from CFB, we elaborated a method to generate emission inventory using the satellite data of “MODIS Thermal Anomalies/Fire product (MOD/MYD14DL)”. The MOD/MYD14DL product detected small opening fires (<100 m²), with daily temporal resolution (Giglio et al., 2003), and located fire activities (van der Werf et al., 2006).

We estimated the CO emission of CFB using the annual provincial statistical data (Streets et al.,
25 2003;Cao et al., 2008;Zhang et al., 2008;Ni et al., 2015). The provincial emission of crop residues burning can be calculated by Eq. (1):

$$E_{i,CO} = P_i \times R \times F_i \times CE \times EF_{CO}, \quad (1)$$

where $E_{i,CO}$ stands for CO emission from CFB of i -th province; P_i is provincial crop production; R is crop-specific-residue-to-production ratio (dry matter); F_i is provincial crop-specific percentage of



crop residues burned in the field; CE is percentage of combustion efficiency; EF_{CO} is the emission factors of CFB.

Furthermore, the CO emission was temporally and spatially allocated according to the CFB activities (Huang et al., 2012), which was defined as MOD/MYD14DL active fires occurred over the cropland
5 classification of the MODIS Combined Land Cover Type product (Friedl et al., 2010). The detailed CO emission of k -th grid (E_k) was calculated using Eq. (2):

$$E_{k,CO} = \frac{FC_k}{FC_i} \times E_{i,CO}, \quad (2)$$

where FC_k is the total fire counts in k -th grid, and FC_i is the total fire counts in i -th province.

Based on the spatial and temporal emission of CO, the emissions of various gaseous and particulate
10 species (E_{spec1}) were calculated by the Eq. (3) and individual chemical compounds (E_{spec2}) were calculated by Eq. (4).

$$E_{k,spec1} = \frac{EF_{spec1}}{EF_{CO}} \times E_{k,CO}, \quad (3)$$

$$E_{k,spec2} = E_{k,NMOC} \times scale, \quad (4)$$

where $E_{k,spec1}$ and $E_{k,spec2}$ are the k -th grid emission of the specify WRF-Chem species; EF_{spec1}
15 and EF_{CO} are the emission factors of CFB; $E_{k,NMOC}$ is the k -th grid emission of NMOC calculated by Eq. (3); $scale$ is the value to convert NMOC emissions to WRF-Chem chemical species. The emission factors for gaseous and particulate species, and scales to convert NMOC emissions to WRF-Chem chemical species from CFB were taken from available datasets (Wiedinmyer et al., 2011; Akagi et al., 2011; Andreae and Merlet, 2001) (see **Table 2**).

20 4 Results and discussions

4.1 Evaluate the Crop field burning emission

The provincial CO emissions of CFB were estimated based on Eq. (1) (see **Supplementary Table S1**).
In order to evaluate the estimate of CFB emissions, we compared our result to previous studies. In our
evaluation, the total CO emission of CFB in China is 8481 Gg in 2012. This result is comparable to
25 previous published results of Cao et al. (2008) for 8241 Gg in 2002 and Huang et al. (2012) for 4360 Gg in 2006.

In this case study, according to the crop fires detected by the MODIS in NCP during the haze episode, a large amount of agriculture residues burning activities occurred in SNCP, including provinces of



Henan with 61% and Shandong with 22% (see **Fig. 3** and **Table 3**). The most burning occurred on the Oct. 6th with 56%, and it decreased to 18% on Oct. 7th (**Table 3**). We obtained the daily CO emission of CFB depending on Eq. (2). **Fig. 3** displays the CFB and related CO emission on Oct. 6th and 7th when the most CFB occurred.

5 Emission of chemical species required by the WRF-Chem model were calculated using Eq. (3) and (4). **Table 4** shows the gaseous and particulate species emissions from CFB on Oct. 6th and 7th, including the mega cities of Beijing and Tianjin, and provinces of Hebei, Henan and Shandong in NCP. Most of the pollutants are emitted from Henan in SNCP, accounting for 73% on Oct. 6th and 65% on Oct. 7th. Large amounts of pollutions emitted from CFB on Oct. 6th, producing more than 5.4 Gg PM_{2.5} and
10 103.9 Gg CO (1 Gg = 10⁹ g).

4.2 Statistical characteristics of the evaluation

The characteristics of the haze pollution was defined by PM_{2.5} concentration, which is significantly affected by the local wind field and PBLH in the NCP region (Tie et al., 2015). In order to evaluate the model performance, the model simulation was intensive compared with the measured results in both
15 PM_{2.5} concentration and meteorological parameters (wind speed, wind direction, and the PBLH). The normalized mean bias (NMB) and correlation coefficient (R) were used to quantify the performance.

$$NMB = \frac{\sum_{i=1}^N (P_i - O_i)}{\sum_{i=1}^N O_i}, \quad (5)$$

$$R = \frac{\sum_{i=1}^N (P_i - \bar{P})(O_i - \bar{O})}{[\sum_{i=1}^N (P_i - \bar{P})^2 \sum_{i=1}^N (O_i - \bar{O})^2]^{1/2}}, \quad (6)$$

where P_i is the predicted results and O_i represents the related observations. N is the total number of
20 the predictions used for comparisons. Meanwhile, \bar{P} and \bar{O} are the average prediction and related mean observation, respectively.

Figure 4 shows the measured and calculated temporal variations of regional averaged PM_{2.5} concentration, wind speed, wind direction and PBLH. The WRF-Chem model reproduced the pollution episode with a good agreement with observations. The correlation coefficients (R) of simulated and
25 measured PM_{2.5} concentration are 0.87 in NNCP and 0.80 in SNCP. The NMB are -14% in NNCP and -3% in SNCP. The relative high NMB of -14% is mainly due to the negative bias in S3, which may be resulted from cloud contamination (**Supplementary Fig. S1**), and it has few impacts on the contribution of the CFB since few open crop fires occurred during that time. The comparisons between



simulated and observed wind fields show good agreements (**Fig. 4b and 4c**), with all the R being higher than 0.65, and the absolute NMB being no more than 15%. In addition, the R of PBLH are larger than 0.88 and the NMB are smaller than 10% in both NNCP and SNCP (**Fig. 4d**).

4.3 Characteristics of the heavy pollution events

- 5 According to the evolution of $PM_{2.5}$ concentration (see **Fig. 4a**), the haze episode can be divided into three stages: (I) pollution formation stage (S1, 12:00 6th - 00:00 8th), (II) pollution outbreak stage (S2, 00:00 8th - 00:00 10th) and (III) pollution clear stage (S3, 00:00 10th - 00:00 12th). The major characteristics of each stage are briefly summarized below. The detailed observations are followed by related simulations in bracket.
- 10 - S1 (pollution formation): It is dominated by a strong southerly wind, with mean wind speed of 2.5 (2.7) $m s^{-1}$ in NNCP and 3.0 (3.6) $m s^{-1}$ in SNCP. The pollution is continuously transported from SNCP to NNCP, leading to pollutants accumulation in NNCP, which is characterized by the steady rising $PM_{2.5}$ concentration in NNCP from 20.6 (39.6) $\mu g m^{-3}$ (at 12:00 Oct. 6th) to 242.7 (218.7) $\mu g m^{-3}$ (at 00:00 Oct. 8th) (**Fig. 4 a1**).
- 15 - S2 (pollution outbreak): The S2 is a relative stable period of heavy pollution with averaged $PM_{2.5}$ concentration of 252.0 (241.4) $\mu g m^{-3}$ in NNCP and 214.1 (235.1) $\mu g m^{-3}$ in SNCP, which are much higher than those in other stages. It was related to relative lower wind speed and PBLH, which are 2.1 (2.2) $m s^{-1}$ and 785 (908) m in NNCP, and 2.5 (2.9) $m s^{-1}$ and 909 (921) m in SNCP.
- S3 (pollution clear): During S3, the southerly gradually decrease, and turn to northerly at the end of
- 20 S3. The clean air from the north region of NNCP obviously improves air quality. Compared with S2, the averaged $PM_{2.5}$ concentrations are both decreased in NNCP and SNCP.

There were several important issues shown in the results, and should be addressed. (1) The $PM_{2.5}$ concentrations are extremely high during the S2 period, and the daily average concentrations are

25 exceed the Chinese National Standard (75 $\mu g m^{-3}$) by 2-3 times. (2) The pollutions are severe in a large region (occurred in both NNCP and SNCP). (3) During the S1 and S2 periods, there is a time lag between SNCP and NNCP for $PM_{2.5}$ concentrations. Because it is a south wind direction, it shows the important impact of long-range transport of $PM_{2.5}$ particles from the SNCP to NNCP.



4.4 Contributions of crop field burning

Model sensitive studies were conducted to separate the individual contribution of CFB on the heavy aerosol pollution. Two model simulations were performed, i.e., one with both anthropogenic and CFB emissions while the other with only anthropogenic emission. We calculated $PM_{2.5}$ distributions by including crop fire emissions (anthropogenic and CFB) and excluding crop field emissions (only anthropogenic). The contributions were quantified by regional averaged contribution in mass concentration ($CMPM_{2.5}$) and daily averaged contribution ratio ($\overline{RPM}_{2.5}$).

$$CMPM_{2.5} = TPM_{2.5} - APM_{2.5}, \quad (7)$$

$$\overline{RPM}_{2.5} = \frac{\overline{CMPM}_{2.5}}{\overline{TPM}_{2.5}}, \quad (8)$$

where $TPM_{2.5}$ represents the simulated $PM_{2.5}$ concentrations considering total emission; $APM_{2.5}$ denotes the simulated $PM_{2.5}$ concentrations only considering anthropogenic emissions. $\overline{CMPM}_{2.5}$ and $\overline{TPM}_{2.5}$ are daily averaged value for $CMPM_{2.5}$ and $TPM_{2.5}$, respectively.

Figure 5 displays the regional observed and simulated $PM_{2.5}$ concentrations considering total emissions (anthropogenic and CFB) and only anthropogenic emissions. It is clearly shown that the CFB had important contributions to $PM_{2.5}$ in both NNCP (**Fig. 5a**) and SNCP (**Fig. 5b**). This is also proved by the daily averaged contribution ratio ($\overline{RPM}_{2.5}$) of CFB (**Table 5**). The high values of $\overline{RPM}_{2.5}$ in SNCP occur on Oct 6th with 35% and on 7th with 17%, when a large amount of CFB happened. Simultaneously, the high values of $\overline{RPM}_{2.5}$ in NNCP occur on Oct 7th with 32% and 8th with 10%, showing a later occurrence (one day-lag) than that in SNCP. The one-day lag suggested that the plume with CFB could be transported from SNCP (where CFB occurred) to NNCP.

The detailed hourly contributions of CFB to $PM_{2.5}$ mass concentration ($CMPM_{2.5}$) are displayed in **Fig. 6**. The values of $CMPM_{2.5}$ in NNCP are generally lag synchronized with that in SNCP, such as P_{N1} versus P_{S1} and P_{N2} versus to P_{S2} (**Fig. 6a and 6b**). Apparently, the lagged time is not constant and varied with the wind field. The specific details performed relaxed lag synchronized, especially the P_{N2} versus to P_{S2} . **Figure 6** further indicates that the CFB contribution in SNCP is mainly due to local emission, while contribution in NNCP is largely resulted from regional transport. Indeed, day-averaged transport contribution to $PM_{2.5}$ from CFB in NNCP can be as high as 32% (see **Table 5**). Such a high transported contribution indicates that the CFB has not only a local pollution, but also has significant



regional impact on air pollution.

Moreover, the $CMPM_{2.5}$ in SNCP drops much faster than that in NNCP (see **P2** in **Fig. 6c**). To clearly show the time evolution of the effect of CFB on $PM_{2.5}$ concentration, four time-points were defined in **Fig. 6c**, such as T1 (23:00 6th), T2 (05:00 7th), T3 (20:00 7th) and T4 (19:00 8th). It shows that at T1, there is a large CFB (in P1), and the $CMPM_{2.5}$ is the highest ($76.1 \mu\text{g m}^{-3}$) in SNCP, but with a low value ($6.2 \mu\text{g m}^{-3}$) in NNCP. At T2, the $CMPM_{2.5}$ is decrease ($53.7 \mu\text{g m}^{-3}$) in SCNP, but has high value ($44.3 \mu\text{g m}^{-3}$) in NNCP (near the transition between P1 and P2). At T3, the $CMPM_{2.5}$ in SNCP rapidly decreased to a low value ($25.6 \mu\text{g m}^{-3}$), but the value is the highest ($48.7 \mu\text{g m}^{-3}$) in NNCP. At T4, the $CMPM_{2.5}$ are low in both SCNP ($8.7 \mu\text{g m}^{-3}$) and NNCP ($11.8 \mu\text{g m}^{-3}$), indicating the effect of CFB largely decreases. The values of $CMPM_{2.5}$ in NNCP are higher than that in SCCP from T3 to T4, indicating the longer effect of CFB on $PM_{2.5}$ concentration in NNCP than in SNCP (in P2).

Figure 7 shows the horizontal distributions of $TPM_{2.5}$ and $CMPM_{2.5}$ at T1, T2, T3 and T4, and the related regional statistical results of $CMPM_{2.5}$ is displayed in **Table 6**. It shows that at T1 the massive local pollutants are emitted from CFB in SNCP and it had not been significantly transported to NNCP. The values of $CMPM_{2.5}$ are high in SNCP with interquartile range of $23\text{-}109 \mu\text{g m}^{-3}$ ([Q1-Q3]), whereas in NNCP, the values of $CMPM_{2.5}$ are low with interquartile range of $0\text{-}10 \mu\text{g m}^{-3}$. At T2, high $CMPM_{2.5}$ values with interquartile range of $10\text{-}60 \mu\text{g m}^{-3}$ remains in both SNCP and NNCP, suggesting that a large amount of CFB pollutants emitted from SNCP and had been transported to NNCP. At T3, values of $CMPM_{2.5}$ rapidly reduce in SNCP with interquartile range of $5\text{-}36 \mu\text{g m}^{-3}$. It is worth to note that the high $CMPM_{2.5}$ values with interquartile range of $28\text{-}72 \mu\text{g m}^{-3}$ are still remained in NNCP. The highest values of $TPM_{2.5}$ are along the foothill of the Taihang Mountains (see **Left panels of Fig.7**), indicating the influence of mountains, and the detailed effects of mountains were analyzed in the following sections. At T4, the pollutants contributed by CFB largely decreases in both SNCP and NNCP. More details about the statistical results of $CMPM_{2.5}$ are shown in **Table 6**.

4.5 Impact of mountains

To clarify the impact of mountains on $PM_{2.5}$ pollution, sensitivity model experiments were conducted to quantify the impacts of the Taihang Mountains (referred as R-T), the Yanshan Mountains (R-Y) and both (R-TY) on the heavy pollution in NCP. We removed the mountains from the model calculation, in



which, the altitude of mountains were reduced to the averaged altitude of NCP (30 m). With the reduction of altitudes of the topography, the dynamical conditions calculated from WRF-Chem changed, which affect pollutions transport, especially along the foothill of mountains. The differences between the simulations with or without mountains showed the net effect of the topography on $PM_{2.5}$ concentration, which was calculated using Eq. (9). And the sensitive configuration and related enclosing scope are displayed in **Supplementary Fig. S2**.

$$IPM_{2.5} = RPM_{2.5} - TPM_{2.5}, \quad (9)$$

where $IPM_{2.5}$ is the net impacts of mountains on $PM_{2.5}$; $RPM_{2.5}$ denotes the simulated $PM_{2.5}$ concentration with removal behaviors, involving R-TY, R-T, and R-Y; $TPM_{2.5}$ represents the simulated $PM_{2.5}$ concentration considering emission of anthropogenic and CFB, which is correspond with the case of R0 (**Supplementary Fig. S2a**).

The sensitive study period was selected from 12:00 7th to 00:00 10th. **Fig. 8** displays the elevation contours and the horizontal distributions of $PM_{2.5}$ concentration with the effect of mountains. The results illustrate that the mountains had important impacts on regional $PM_{2.5}$ concentration, especially the region along the foothill of mountains with a heavy pollution area, covering sampling sites of BJ, BD, SJZ and XT. Here, we summarized two categories of mountain effects, including: (1) In NCP, the Taihang Mountains is a major southwest-northeast mountain and the Yanshan Mountains is a major west-east mountain, when the wind blows from south to north or southeast to northwest, it is often blocked at the foothill of mountains, resulting in the high $PM_{2.5}$ loading (*mountain blocking effect*). (2) When the prevailing winds are south-north or southeast-northwest, the Taihang Mountains act as a transmission guider oriented pollution accumulation along the foothill downwind areas (*mountain guiding effect*). Both effects act to prevent the pollutant plume to disperse toward west of mountains, causing accumulations of the air pollutants along the foothill of mountains. These two mountain effects are illustrated as the schematic pictures in **Supplementary Fig. S3**. The mountain effects were quantified by the averaged horizontal distribution of $PM_{2.5}$ concentration.

Fig. 9 displays the simulated $PM_{2.5}$ concentration due to the mountain effects ($RPM_{2.5}$), with the three cases (R-TY, R-T, and R-Y). The previous heavy pollution accumulation (**shown in Fig. 8**) along the foothill of mountains is significantly reduced, especially with the removal of Taihang Mountains (R-T, and RTY) (see **Fig. 9 a1** and **a2**). In these two cases, the pollution plumes dispersed westerly (see **Fig. 9 b1** and **b2**). It shows that the $PM_{2.5}$ concentrations increased 40-120 $\mu\text{g m}^{-3}$ in the western part of



Taihang Mountains, and reduced 20-60 $\mu\text{g m}^{-3}$ in NCP. The distribution of the reduced pollution plume shows a northeast band plume, indicating both the mountain blocking and guiding effects. With the case of removal the Yanshan Mountains (R-Y), the high $\text{PM}_{2.5}$ concentrations are still remained along the foothill of the Taihang Mountains (see Fig. 9 a3), but more pollutants are guided along the foothill to the northeastern of NCP. Without the blocking effect of the Yanshan Mountains, the $\text{PM}_{2.5}$ concentrations increased 20-80 $\mu\text{g m}^{-3}$ in the northern part of the Yanshan Mountains, and decreased 10-60 $\mu\text{g m}^{-3}$ in the southern part of the Yanshan Mountains (see Fig. 9 b3).

In the foothill sampling sites (BJ, BD, SJZ and XT), the averaged $\text{PM}_{2.5}$ concentrations are reduced 56.0 $\mu\text{g m}^{-3}$ for the case of R-T, which is much higher than the case of R-Y (25.1 $\mu\text{g m}^{-3}$). For the other non-foothill sites, the averaged reduction is 36.1 $\mu\text{g m}^{-3}$ for the case of R-T, which is also much higher than the case of R-Y (1.3 $\mu\text{g m}^{-3}$), suggesting that the Taihang Mountains have stronger effects than the Yanshan Mountains. The higher impacts in the foothill sampling sites than non-foothill sites are further demonstrated, including blocking and guiding effects of mountains on $\text{PM}_{2.5}$ pollutions in NCP.

5 Conclusions

In recent years, the NCP region, including the capital city of Beijing, has been suffering serious haze pollution problem, causing by multiply emissions. One of the causes is due to the CFB, which had not been carefully studied. In this study, we extracted a more detailed emission inventory of CFB based on the provincial statistical data and open crop fires captured by satellite (MODIS). A regional dynamical/chemical model (WRF-Chem) was applied to study the effect of CFB on the $\text{PM}_{2.5}$ concentrations in NCP. The results are summarized:

- (1) In order to intensive performance of the model studies, the model simulations were intensive compared with the measured results in both $\text{PM}_{2.5}$ concentrations and meteorological parameters (wind speed, wind direction, and the PBLH). The WRF-Chem model reproduced the pollution episode with a good agreement with observations. The correlation coefficients (R) of simulated and measured $\text{PM}_{2.5}$ concentration are 0.87 in NNCP and 0.80 in SNCP, and the related NMB are -14% in NNCP and -3% in SNCP. The simulated meteorological parameters (winds and PBLH) are also in good agreement with observations in both NNCP and SNCP.
- (2) The CFB performs important contribution to $\text{PM}_{2.5}$ concentration and the maximum daily



averaged contributions are higher than 32% in both SNCP and NNCP. The contribution in SNCP is mainly due to local emission, whereas contribution in NNCP is largely resulted from regional transport.

- (3) The research domain includes two important areas. One is the north part of NCP (NNCP), including two mega cities (Beijing and Tianjin), where only few CFB occurred. Another is the south part of the NCP (SNCP), where substantial crop fires occurred during the haze episodes. Because of the haze problem in the capital city of China (Beijing), one of the main focuses is to study the long-range transport of CFB from SNCP to NNCP. This study shows that there are substantially long-transport of CFB plume from SNCP to NNCP. More importantly, the effect of CFB remains in a longer time in NNCP than in SNCP along the foothill of the Taihang Mountains, causing significant enhancement in Beijing in both time and magnitude.
- (4) Another major finding is that the mountains played significant roles in affecting the $PM_{2.5}$ pollution through the blocking effect and guiding effect. With the reduction of the topography altitudes, the dynamical conditions calculated from WRF-Chem change, which affect pollutions transport, especially along the foothill of mountains. The mountain blocking effect represents the phenomenon that pollutants are often blocked and then resulted in $PM_{2.5}$ accumulation at the foothill of mountains. The mountain guiding effect denotes the mountains act as a transmission guider oriented pollution accumulation along the foothill downwind areas.

This study suggests that the $PM_{2.5}$ emissions in the southern NCP should be significantly limited in order to reduce the occurrences of heavy haze events in NNCP region, including the Beijing City.

Acknowledgement

The PBL height and wind field data was obtained from the European Centre for Medium-Range Weather Forecasts (ECMWF) website (<http://www.ecmwf.int/products/data/>). This work is supported by the National Natural Science Foundation of China (NSFC) under Grant Nos. 41275186 and 41430424, and the Open Fund of the State Key Laboratory of Loess and Quaternary Geology (SKLLQG1413). The National Center for Atmospheric Research is sponsored by the National Science Foundation.



Reference

- Akagi, S., Yokelson, R. J., Wiedinmyer, C., Alvarado, M., Reid, J., Karl, T., Crouse, J., and Wennberg, P.: Emission factors for open and domestic biomass burning for use in atmospheric models, *Atmospheric Chemistry and Physics*, 11, 4039-4072, 2011.
- 5 Andreae, M. O., and Merlet, P.: Emission of trace gases and aerosols from biomass burning, *Global biogeochemical cycles*, 15, 955-966, 2001.
- Binkowski, F. S., and Roselle, S. J.: Models - 3 Community Multiscale Air Quality (CMAQ) model aerosol component 1. Model description, *Journal of Geophysical Research: Atmospheres*, 108, 2003.
- 10 Cao, G., Zhang, X., Wang, Y., and Zheng, F.: Estimation of emissions from field burning of crop straw in China, *Chinese Science Bulletin*, 53, 784-790, 2008.
- Chang, J., Brost, R., Isaksen, I., Madronich, S., Middleton, P., Stockwell, W., and Walcek, C.: A three - dimensional Eulerian acid deposition model: Physical concepts and formulation, *Journal of Geophysical Research: Atmospheres (1984–2012)*, 92, 14681-14700, 1987.
- 15 Chen, F., and Dudhia, J.: Coupling an advanced land surface-hydrology model with the Penn State-NCAR MM5 modeling system. Part I: Model implementation and sensitivity, *Monthly Weather Review*, 129, 569-585, 2001.
- Cheng, Y., Engling, G., He, K.-B., Duan, F.-K., Ma, Y.-L., Du, Z.-Y., Liu, J.-M., Zheng, M., and Weber, R. J.: Biomass burning contribution to Beijing aerosol, *Atmospheric Chemistry and*
20 *Physics*, 13, 7765-7781, 2013.
- Cheng, Z., Wang, S., Fu, X., Watson, J., Jiang, J., Fu, Q., Chen, C., Xu, B., Yu, J., and Chow, J.: Impact of biomass burning on haze pollution in the Yangtze River delta, China: a case study in summer 2011, *Atmospheric Chemistry and Physics*, 14, 4573-4585, 2014.
- Dudhia, J.: Numerical study of convection observed during the winter monsoon experiment using a
25 mesoscale two-dimensional model, *Journal of the Atmospheric Sciences*, 46, 3077-3107, 1989.
- Emmons, L., Walters, S., Hess, P., Lamarque, J.-F., Pfister, G., Fillmore, D., Granier, C., Guenther, A., Kinnison, D., and Laepple, T.: Description and evaluation of the Model for Ozone and Related chemical Tracers, version 4 (MOZART-4), *Geoscientific Model Development*, 3, 43-67, 2010.
- Friedl, M. A., Sulla-Menashe, D., Tan, B., Schneider, A., Ramankutty, N., Sibley, A., and Huang, X.:
30 MODIS Collection 5 global land cover: Algorithm refinements and characterization of new datasets, *Remote Sensing of Environment*, 114, 168-182, 2010.
- Giglio, L., Descloitres, J., Justice, C. O., and Kaufman, Y. J.: An enhanced contextual fire detection algorithm for MODIS, *Remote sensing of environment*, 87, 273-282, 2003.
- Guenther, A., Zimmerman, P., and Wildermuth, M.: Natural volatile organic compound emission rate
35 estimates for US woodland landscapes, *Atmospheric Environment*, 28, 1197-1210, 1994.
- He, H., Tie, X., Zhang, Q., Liu, X., Gao, Q., Li, X., and Gao, Y.: Analysis of the causes of heavy aerosol pollution in Beijing, China: A case study with the WRF-Chem model, *Particology*, 20, 32-40, 2015a.
- He, M., Zheng, J., Yin, S., and Zhang, Y.: Trends, temporal and spatial characteristics, and
40 uncertainties in biomass burning emissions in the Pearl River Delta, China, *Atmospheric Environment*, 45, 4051-4059, 2011.
- He, Q., Zhao, X., Lu, J., Zhou, G., Yang, H., Gao, W., Yu, W., and Cheng, T.: Impacts of biomass-burning on aerosol properties of a severe haze event over Shanghai, *Particology*, 20, 52-60, 2015b.



- Hong, S.-Y., Noh, Y., and Dudhia, J.: A new vertical diffusion package with an explicit treatment of entrainment processes, *Monthly Weather Review*, 134, 2318-2341, 2006.
- Huang, X., Li, M., Li, J., and Song, Y.: A high-resolution emission inventory of crop burning in fields in China based on MODIS Thermal Anomalies/Fire products, *Atmospheric Environment*, 50, 9-15, 2012.
- 5 Jiang, C., Wang, H., Zhao, T., Li, T., and Che, H.: Modeling study of PM 2.5 pollutant transport across cities in China's Jing-Jin-Ji region during a severe haze episode in December 2013, *Atmospheric Chemistry and Physics*, 15, 5803-5814, 2015.
- Li, W., Shao, L., and Buseck, P.: Haze types in Beijing and the influence of agricultural biomass burning, *Atmospheric Chemistry and Physics*, 10, 8119-8130, 2010.
- 10 Lin, Y.-L., Farley, R. D., and Orville, H. D.: Bulk parameterization of the snow field in a cloud model, *Journal of Climate and Applied Meteorology*, 22, 1065-1092, 1983.
- Madronich, S., and Flocke, S.: The role of solar radiation in atmospheric chemistry, in: *Environmental photochemistry*, Springer, 1-26, 1999.
- 15 Mlawer, E. J., Taubman, S. J., Brown, P. D., Iacono, M. J., and Clough, S. A.: Radiative transfer for inhomogeneous atmospheres: RRTM, a validated correlated-k model for the longwave (Paper 97JD00237), *JOURNAL OF GEOPHYSICAL RESEARCH-ALL SERIES-*, 102, 16,663-616,682, 1997.
- Ni, H., Han, Y., Cao, J., Chen, L.-W. A., Tian, J., Wang, X., Chow, J. C., Watson, J. G., Wang, Q., and Wang, P.: Emission characteristics of carbonaceous particles and trace gases from open burning of crop residues in China, *Atmospheric Environment*, 2015.
- 20 Stockwell, W. R., Middleton, P., Chang, J. S., and Tang, X.: The second generation regional acid deposition model chemical mechanism for regional air quality modeling, *Journal of Geophysical Research: Atmospheres* (1984–2012), 95, 16343-16367, 1990.
- 25 Streets, D., Yarber, K., Woo, J. H., and Carmichael, G.: Biomass burning in Asia: Annual and seasonal estimates and atmospheric emissions, *Global Biogeochemical Cycles*, 17, 2003.
- Tie, X., Madronich, S., Walters, S., Zhang, R., Rasch, P., and Collins, W.: Effect of clouds on photolysis and oxidants in the troposphere, *Journal of Geophysical Research: Atmospheres* (1984–2012), 108, 2003.
- 30 Tie, X., Madronich, S., Walters, S., Edwards, D. P., Ginoux, P., Mahowald, N., Zhang, R., Lou, C., and Brasseur, G.: Assessment of the global impact of aerosols on tropospheric oxidants, *Journal of Geophysical Research: Atmospheres* (1984–2012), 110, 2005.
- Tie, X., Madronich, S., Li, G., Ying, Z., Zhang, R., Garcia, A. R., Lee-Taylor, J., and Liu, Y.: Characterizations of chemical oxidants in Mexico City: A regional chemical dynamical model (WRF-Chem) study, *Atmospheric Environment*, 41, 1989-2008, 2007.
- 35 Tie, X., Geng, F., Peng, L., Gao, W., and Zhao, C.: Measurement and modeling of O₃ variability in Shanghai, China: Application of the WRF-Chem model, *Atmospheric Environment*, 43, 4289-4302, 2009.
- Tie, X., Zhang, Q., He, H., Cao, J., Han, S., Gao, Y., Li, X., and Jia, X. C.: A budget analysis of the formation of haze in Beijing, *Atmospheric Environment*, 100, 25-36, 2015.
- 40 van der Werf, G. R., Randerson, J. T., Giglio, L., Collatz, G. J., Kasibhatla, P. S., and Arellano Jr, A. F.: Interannual variability in global biomass burning emissions from 1997 to 2004, *Atmospheric Chemistry and Physics*, 6, 3423-3441, 2006.
- Wang, L., Xu, J., Yang, J., Zhao, X., Wei, W., Cheng, D., Pan, X., and Su, J.: Understanding haze



- pollution over the southern Hebei area of China using the CMAQ model, *Atmospheric Environment*, 56, 69-79, 2012.
- Wang, L., Wei, Z., Yang, J., Zhang, Y., Zhang, F., Su, J., Meng, C., and Zhang, Q.: The 2013 severe haze over southern Hebei, China: model evaluation, source apportionment, and policy implications, *Atmos. Chem. Phys.*, 14, 3151-3173, 2013.
- Wang, Q., Shao, M., Liu, Y., William, K., Paul, G., Li, X., Liu, Y., and Lu, S.: Impact of biomass burning on urban air quality estimated by organic tracers: Guangzhou and Beijing as cases, *Atmospheric Environment*, 41, 8380-8390, 2007.
- Wesely, M.: Parameterization of surface resistances to gaseous dry deposition in regional-scale numerical models, *Atmospheric Environment (1967)*, 23, 1293-1304, 1989.
- Wiedinmyer, C., Akagi, S., Yokelson, R. J., Emmons, L., Al-Saadi, J., Orlando, J., and Soja, A.: The Fire INventory from NCAR (FINN): A high resolution global model to estimate the emissions from open burning, *Geoscientific Model Development*, 4, 625, 2011.
- Yan, X., Ohara, T., and Akimoto, H.: Bottom-up estimate of biomass burning in mainland China, *Atmospheric Environment*, 40, 5262-5273, 2006.
- Yang, Y., Liu, X., Qu, Y., An, J., Jiang, R., Zhang, Y., Sun, Y., Wu, Z., Zhang, F., and Xu, W.: Characteristics and formation mechanism of continuous hazes in China: a case study during the autumn of 2014 in the North China Plain, *Atmospheric Chemistry and Physics*, 15, 8165-8178, 2015.
- Yevich, R., and Logan, J. A.: An assessment of biofuel use and burning of agricultural waste in the developing world, *Global biogeochemical cycles*, 17, 2003.
- Zhang, H., Ye, X., Cheng, T., Chen, J., Yang, X., Wang, L., and Zhang, R.: A laboratory study of agricultural crop residue combustion in China: Emission factors and emission inventory, *Atmospheric Environment*, 42, 8432-8441, 2008.
- Zhang, Q., Streets, D. G., Carmichael, G. R., He, K. B., Huo, H., Kannari, A., Klimont, Z., Park, I. S., Reddy, S., Fu, J. S., Chen, D., Duan, L., Lei, Y., Wang, L. T., and Yao, Z. L.: Asian emissions in 2006 for the NASA INTEX-B mission, *Atmospheric Chemistry and Physics*, 9, 5131-5153, 2009.
- Zhang, Y.-L., and Cao, F.: Is it time to tackle PM 2.5 air pollutions in China from biomass-burning emissions?, *Environmental Pollution*, 202, 217-219, 2015.
- Zhang, Z., Engling, G., Lin, C.-Y., Chou, C. C.-K., Lung, S.-C. C., Chang, S.-Y., Fan, S., Chan, C.-Y., and Zhang, Y.-H.: Chemical speciation, transport and contribution of biomass burning smoke to ambient aerosol in Guangzhou, a mega city of China, *Atmospheric Environment*, 44, 3187-3195, 2010.

35



Figure Captions

- Figure 1** The study area, sampling sites and crop field burning. **(a)** The research domain and related provinces in China. **(b)** Topographical conditions of North China Plain. **(c)** Location of sampling sites and crop field burning captured by MODIS during the haze episodes. Green crosses indicate the measurement sites, and the crop field burning is shown by the pink dots.
- Figure 2** The **(a)** yearly and **(b)** monthly crop field burning observed by MODIS in the research domain during the year of 2006 to 2014.
- Figure 3** Crop field burning captured by MODIS with the background of MODIS real-time true color map **(Left)** and related CO emission **(Right)** on Oct. 6th and 7th.
- Figure 4** Regional averaged temporal variations in simulated and observed results of **(a)** PM_{2.5} concentration, **(b)** wind speed, **(c)** wind direction and **(d)** PBLH over the regions of NNCP and SNCP.
- Figure 5** Hourly PM_{2.5} concentration of observations **(obs)** and simulations **(sim-total and sim-anthro)** in **(a)** NNCP and **(b)** SNCP. **Sim-total** represents the simulations considering total emissions (anthropologic and crop field burning), whereas **sim-anthro** is the simulations only considering anthropologic emissions.
- Figure 6** Hourly contribution of crop field burning to PM_{2.5} mass concentration (*CMPM_{2.5}*) **(a)** in SNCP, **(b)** in NNCP and **(c)** their comparison. The key point-in-local-times of T1 (23:00 6th), T2 (05:00 7th), T3 (20:00 7th) and T4 (19:00 8th) are signed with blue arrow.
- Figure 7** The distributions of *TPM_{2.5}* and *CMPM_{2.5}* of the key point-in-local-times of T1, T2, T3 and T4, which represent different pollution phase of emission from crop field burning to PM_{2.5}.
- Figure 8** The elevation contours and the averaged spatial distributions of horizontal winds and averaged *TPM_{2.5}* during 12:00 7th to 00:00 10th. The point symbols of circles and squares were used to distinguish observation sites weather or not located at the foothill of mountains. Meanwhile, the 200-meter contour was highlighted with bold black line.
- Figure 9** The averaged spatial distribution of PM_{2.5} concentration and horizontal winds during 12:00 7th to 00:00 10th. **(a)** Simulated PM_{2.5} loading with removal behaviors (*RPM_{2.5}*), involving R-TY, R-T, and R-Y. **(b)** The related impacts of mountains to PM_{2.5} (*IPM_{2.5}*), which represents the net effect of related mountains. The bold black lines were used to stress enclosing scope of each removal behavior.



Table 1. The average $PM_{2.5}$ concentration, wind direction and wind speed of the observations from 12:00 6th to 00:00 12th. The sampling sites located at the foot of mountains were emphasized with bold style.

Region	Site	Longitude (°E)	Latitude (°N)	$PM_{2.5}$ ($\mu\text{g}/\text{m}^3$)	Wind-dir (°)	Wind-sp (m/s)
	Beijing (BJ)	116.41	40.04	245.5	185.8	2.2
	Langfang (LF)	116.73	39.56	214.7	177.0	2.4
	Tianjin (TJ)	117.31	39.09	134.7	173.5	2.4
	Baoding (BD)	115.49	38.87	287.7	171.2	2.2
	Cangzhou (CZ)	116.87	38.31	117.3	166.6	2.5
NNCP				200.0	174.8	2.35
	Shijiazhuang (SJZ)	114.49	38.04	257.9	175.2	2.0
	Hengshui (HS)	115.68	37.74	166.7	163.7	2.6
	Dezhou (DZ)	116.31	37.47	152.4	162.7	2.6
	Xingtai (XT)	114.50	37.09	320.1	198.1	2.3
	Liaocheng (LC)	116.00	36.46	139.7	158.4	2.6
	Hezhe (HZ)	115.46	35.26	105.0	138.9	2.4
	Zhengzhou (ZZ)	113.66	34.79	146.9	159.2	2.4
SNCP				184.1	165.2	2.42



Table 2. The gaseous and particulate species emission factors (g/kg) and scales to convert NMOC emissions (kg day^{-1}) to WRF/Chem chemical species ($\text{moles-species day}^{-1}$) from crop field burning. The detailed chemical species are described by Stockwell et al. (1990).

Gaseous species							Particulate species					
CO ¹	NO _x ¹	NO ¹	NO ₂ ²	SO ₂ ³	NH ₃ ¹	NMOC ¹	OC ³	BC ³	PM _{2.5} ¹			
111	3.5	1.7	3.9	0.4	2.3	57	3.3	0.69	5.8			
Chemical-compounds-to-NMOC scales ^{1,2}												
ETH	HC3	HC5	OL2	OLT	OLI	TOL	CSL	HCHO	ALD	KET	ORA2	ISO
0.43	0.73	0.07	1.09	0.27	0.20	1.07	0.49	1.84	3.05	0.83	2.19	0.60

¹ Andreae and Merlet (2001)

5 ² Wiedinmyer et al., (2001)

³ Akagi et al., (2011)



Table 3. The fire counts of crop field burning detected by the MODIS in the provinces over NCP during the haze episode (from Oct. 6th to 11th, 2014)

Province	6-Oct	7-Oct	8-Oct	9-Oct	10-Oct	11-Oct	Percentage
Beijing	0	0	0	0	0	0	0%
Tianjin	0	0	0	0	0	0	0%
Hebei	60	11	14	1	5	6	10%
Henan	370	104	59	18	19	23	61%
Shandong	100	54	9	9	32	7	22%
Anhui	6	6	20	0	10	3	5%
Shanxi	3	0	0	3	4	1	1%
Jiangsu	4	3	5	0	3	1	2%
Percentage	56%	18%	11%	3%	8%	4%	100%



Table 4. The emissions (Gg/day) of gaseous and particulate species from crop field burning on Oct. 6th and Oct. 7th in NCP region, including the provinces of Beijing, Tianjin, Hebei, Henan, Shandong.

Time	Province	CO	NO _x	NO	NO ₂	NMOC	SO ₂	NH ₃	PM _{2.5}	OC	BC
6-Oct	Beijing	0.00	0.00	0.00	0.00	0.00	0.00	0.00	0.00	0.00	0.00
	Tianjin	0.00	0.00	0.00	0.00	0.00	0.00	0.00	0.00	0.00	0.00
	Hebei	10.73	0.34	0.16	0.38	5.51	0.04	0.22	0.56	0.32	0.07
	Henan	75.87	2.39	1.16	2.67	38.96	0.27	1.57	3.96	2.26	0.47
	Shandong	17.35	0.55	0.27	0.61	8.91	0.06	0.36	0.91	0.52	0.11
	Total	103.9	3.3	1.6	3.7	53.4	0.4	2.2	5.4	3.1	0.6
7-Oct	Beijing	0.00	0.00	0.00	0.00	0.00	0.00	0.00	0.00	0.00	0.00
	Tianjin	0.00	0.00	0.00	0.00	0.00	0.00	0.00	0.00	0.00	0.00
	Hebei	1.97	0.06	0.03	0.07	1.01	0.01	0.04	0.10	0.06	0.01
	Henan	21.32	0.67	0.33	0.75	10.95	0.08	0.44	1.11	0.63	0.13
	Shandong	9.37	0.30	0.14	0.33	4.81	0.03	0.19	0.49	0.28	0.06
	Total	32.7	1.0	0.5	1.1	16.8	0.1	0.7	1.7	1.0	0.2



Table 5. Averaged contribution ration of crop field burning to $PM_{2.5}$ concentration

Region	6-Oct.	7-Oct.	8-Oct.	9-Oct.	10-Oct.	11-Oct.
NNCP	4%	32%	10%	3%	2%	4%
SNCP	35%	17%	6%	3%	1%	1%



Table 6. The regional statistical results of crop field burning contribution in mass concentration of $PM_{2.5}$ (μg) for the four time-points of T1 (23:00 6th), T2 (05:00 7th), T3 (20:00 7th) and T4 (19:00 8th).

Region	T1	T2	T3	T4
Mean value of $CMPM_{2.5}$				
NNCP	7.7	37.0	52.8	14.2
SNCP	77.0	38.7	21.6	9.8
Maximum value of $CMPM_{2.5}$				
NNCP	68.2	154.2	127.4	55.7
SNCP	340.5	170.8	81.5	126
First quartile (Q1) of $CMPM_{2.5}$				
NNCP	0.2	9.5	28.4	5.5
SNCP	23.2	10.6	4.6	1.8
Third quartile (Q3) of $CMPM_{2.5}$				
NNCP	10.1	52.2	71.7	21.1
SNCP	109.3	57.6	35.6	8.6

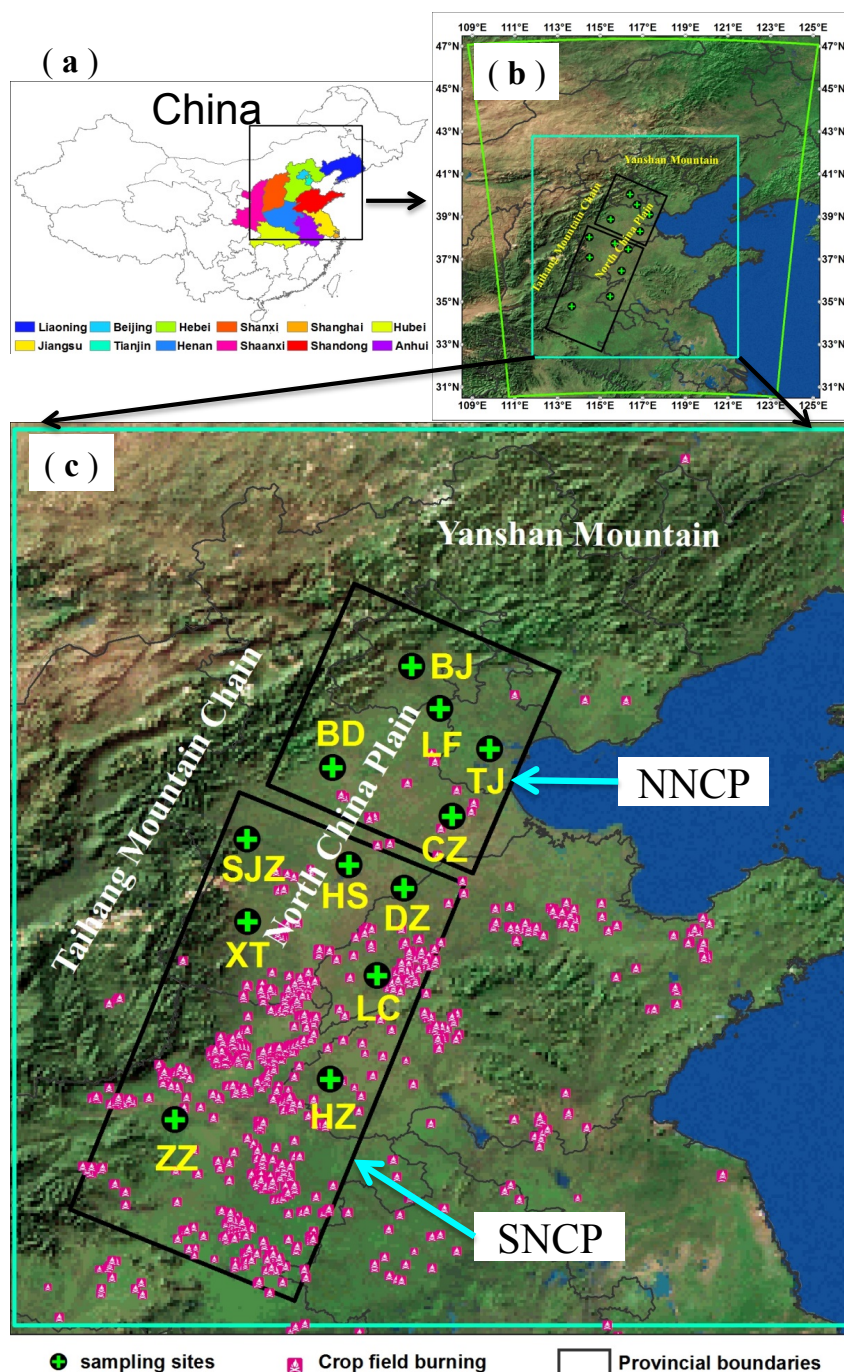


Figure 1

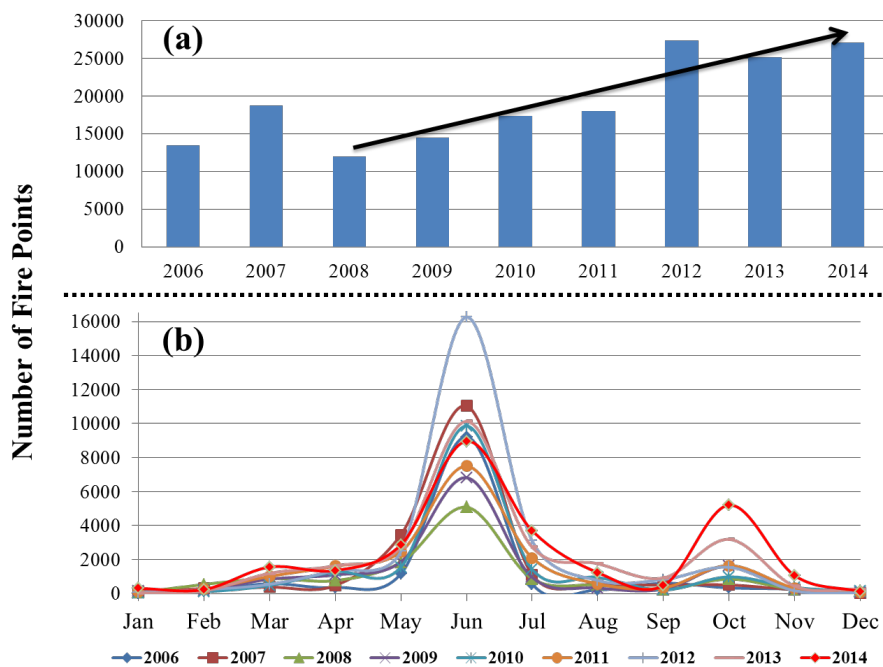


Figure 2

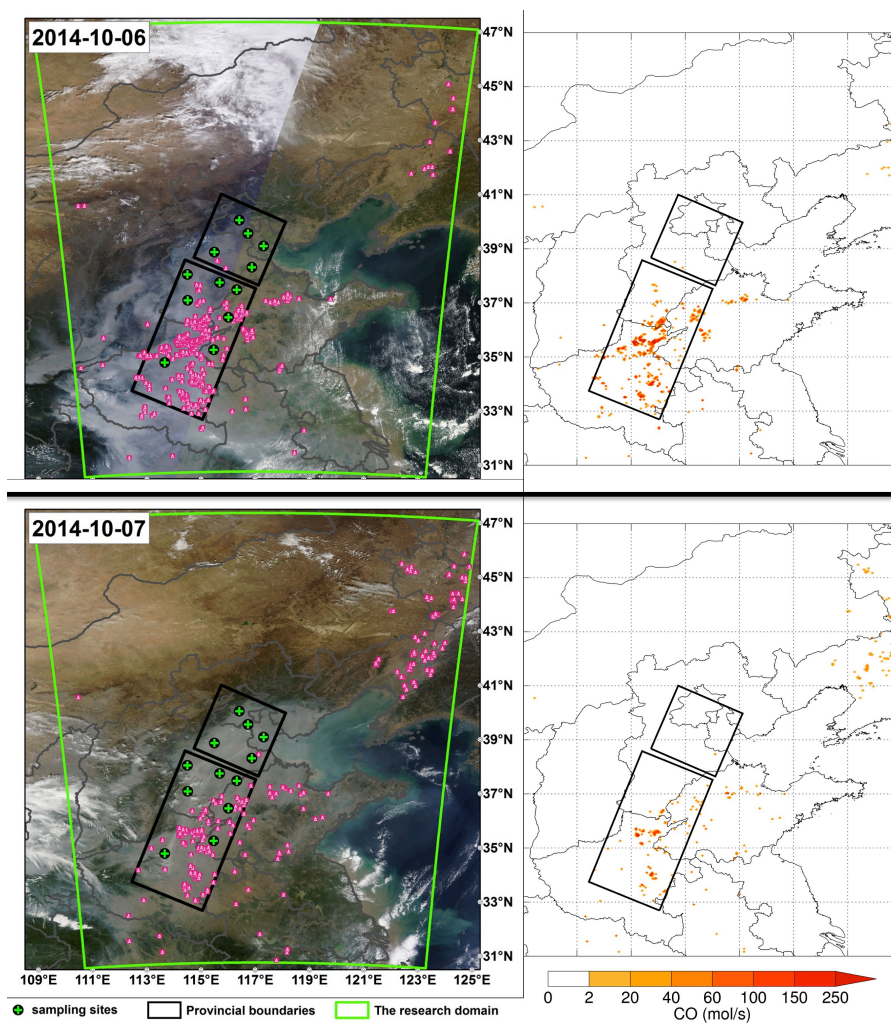


Figure 3

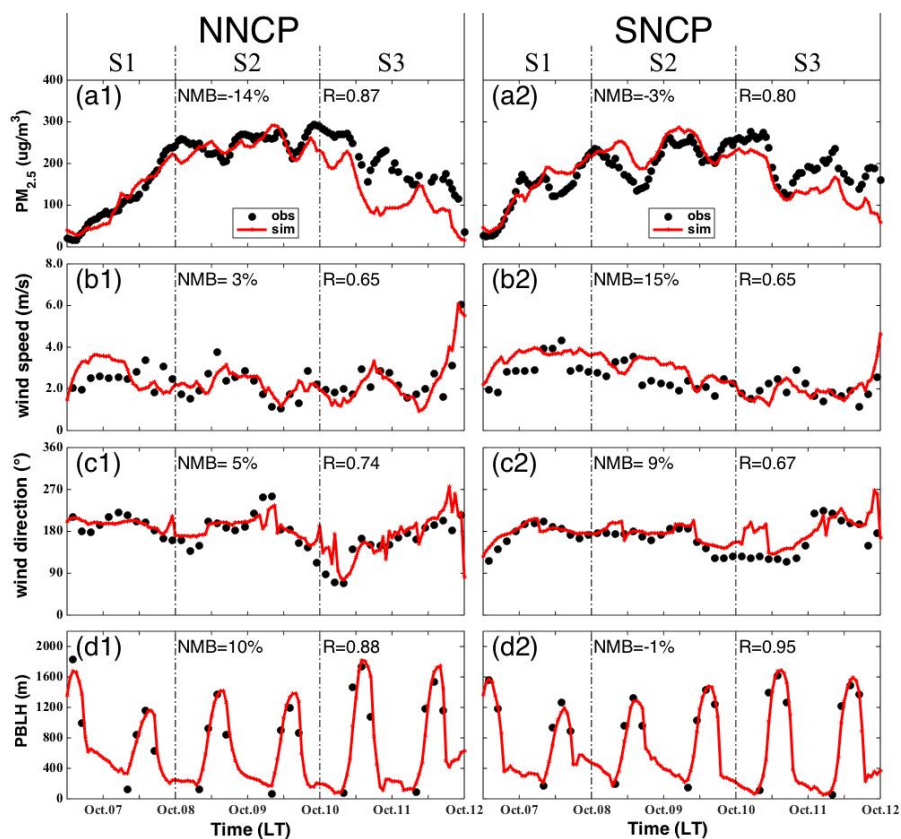


Figure 4

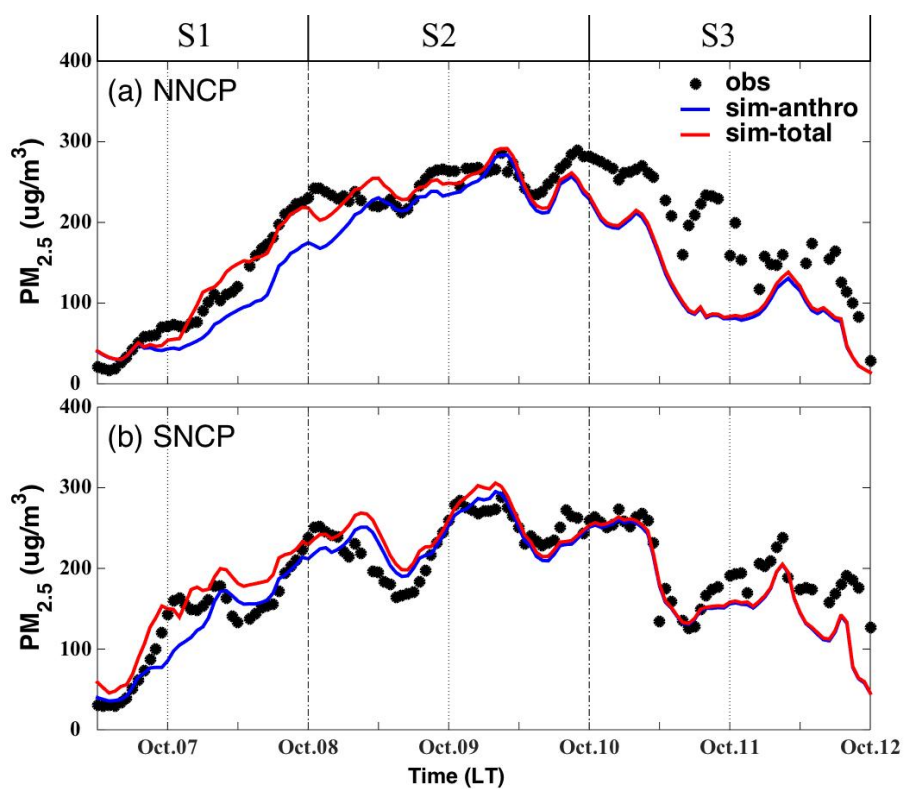


Figure 5

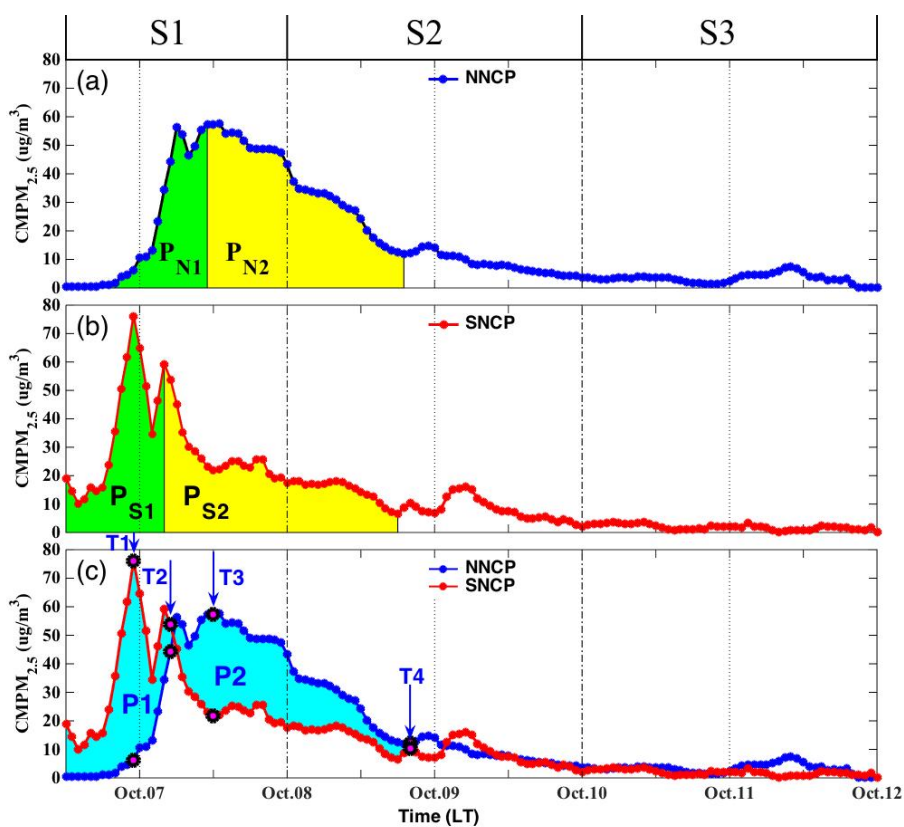


Figure 6

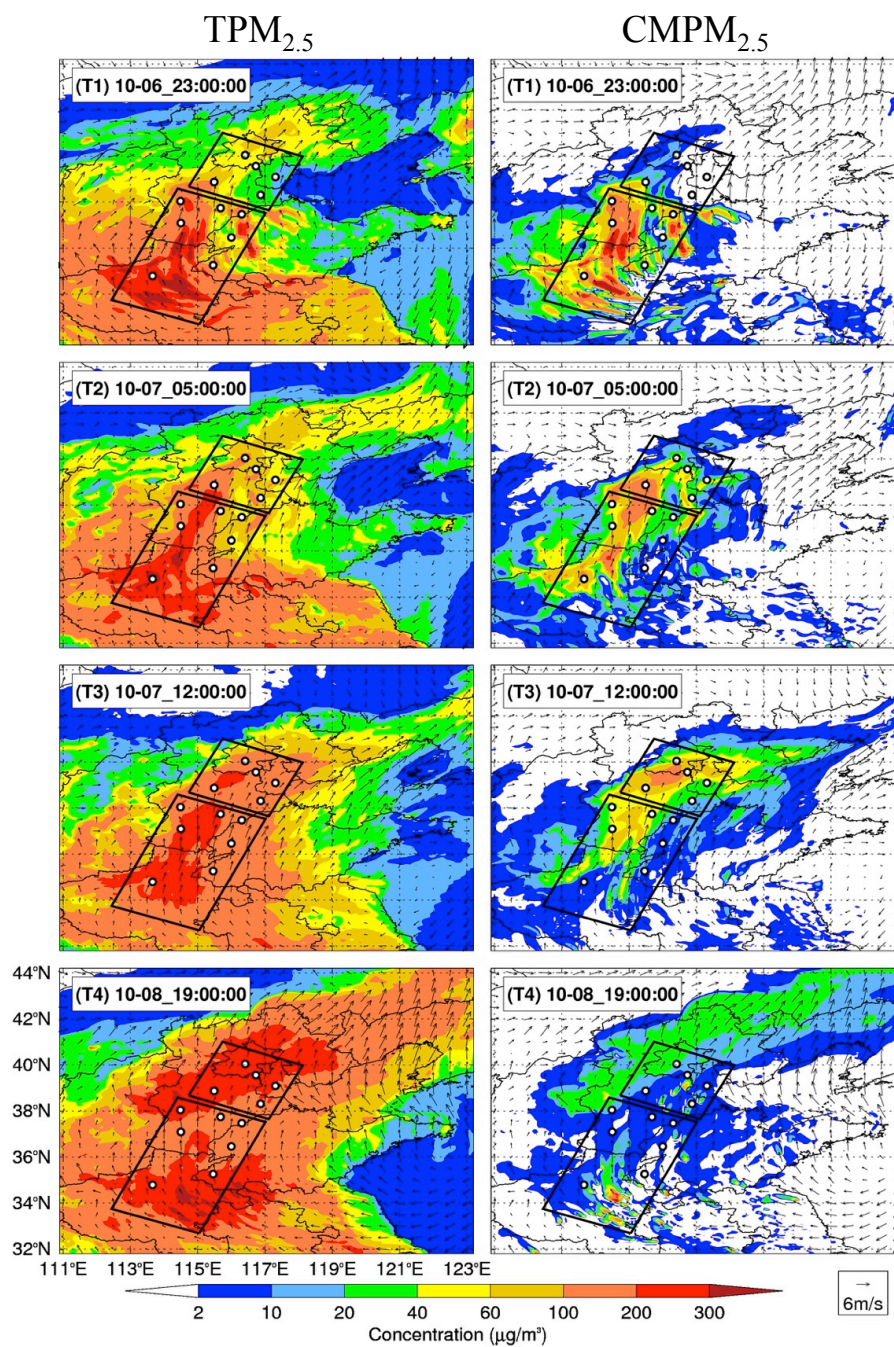


Figure 7

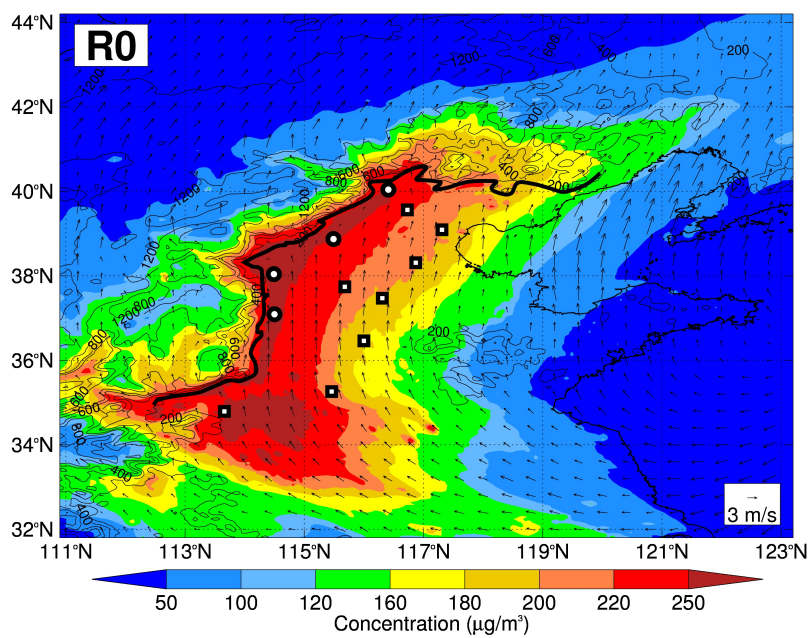


Figure 8

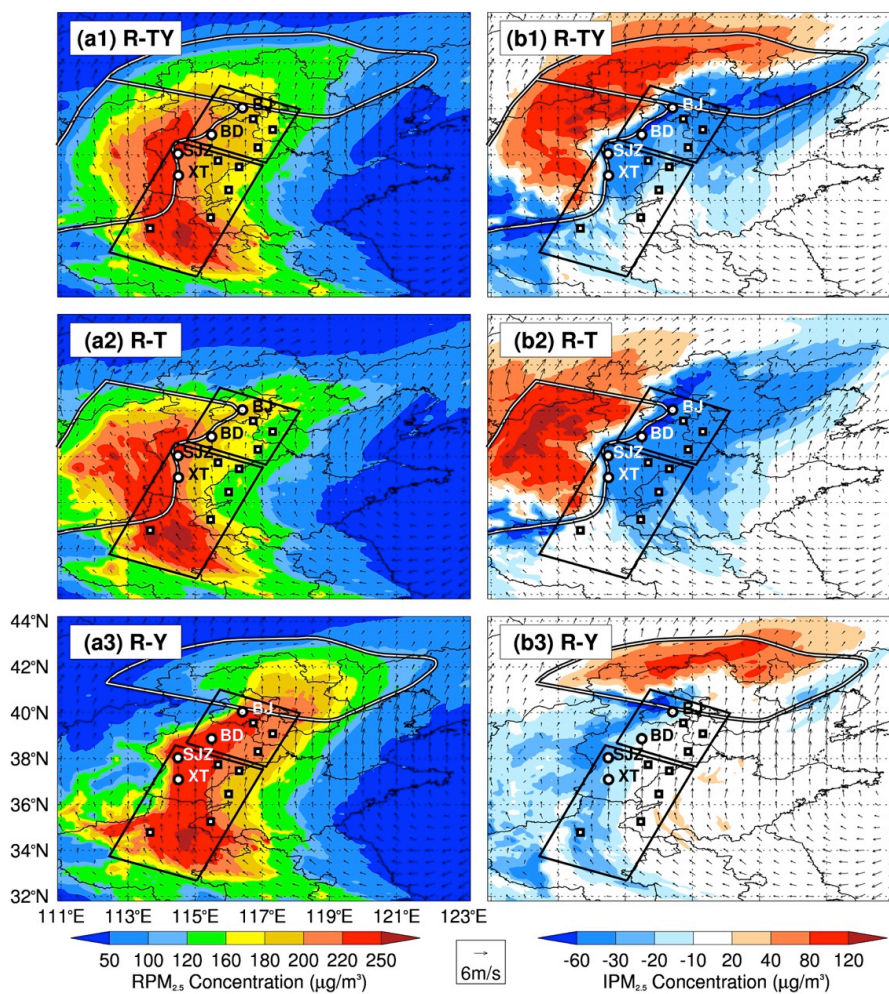


Figure 9